Bone 155 (2022) 116261

Contents lists available at ScienceDirect

Bone

journal homepage: www.elsevier.com/locate/bone

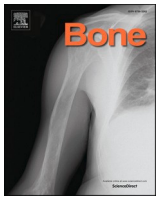

Full Length Article

Bone fragility via degradation of bone quality featured by collagen/apatite micro-arrangement in human rheumatic arthritis

Ryosuke Ozasa [a,1], Aira Matsugaki [a,1], Takuya Ishimoto [a,1], Satoshi Kamura [b], Hiroto Yoshida [c], Mayu Magi [c], Yoshihiro Matsumoto [c], Koji Sakuraba [b], Kenjiro Fujimura [b], Hisaaki Miyahara [b], Takayoshi Nakano [a,*]

[a] Division of Materials and Manufacturing Science, Graduate School of Engineering, Osaka University, 2-1 Yamadaoka, Suita, Osaka 565-0871, Japan
[b] Department of Orthopaedic Surgery, National Hospital Organization, Kyushu Medical Center, 1-8-1 Jigyouhama chuo-ku, Fukuoka, Fukuoka 811-1395, Japan
[c] Product Research Department, Kamakura Research Laboratories, Chugai Pharmaceutical Co., Ltd., 200 Kajiwara, Kamakura, Kanagawa 247-8530, Japan

ARTICLE INFO

Keywords:
Rheumatoid arthritis
Fracture risk assessment
Bone quality
Collagen/apatite orientation
Human knee joint
Osteocyte
Interleukin-6

ABSTRACT

Although increased bone fragility is a well-recognized consequence in patients with rheumatoid arthritis (RA), the essential cause of degenerate bone strength remains unknown. This study aimed to determine factors contributing to bone dysfunction in RA by focusing on the bone matrix micro-arrangement, based on the preferential orientation of collagen and the related apatite *c*-axis as a bone quality index. The classical understanding of RA is limited to its severe pathological conditions associated with inflammation-induced bone loss. This study examined periarticular proximal tibiae from RA patients as compared with osteoarthritis (OA) patients as controls. Bone tissue material strength was disrupted in the RA group compared with the control. Collagen/apatite micro-arrangement and vBMD were significantly lower in the RA group, and the rate of decrease in apatite *c*-axis orientation (−45%) was larger than that in vBMD (−22%). Multiple regression analysis showed that the degree of apatite *c*-axis orientation ($\beta = 0.52$, $p = 1.9 \times 10^{-2}$) significantly contributed to RA-induced bone material impairment as well as vBMD ($\beta = 0.46$, $p = 3.8 \times 10^{-2}$). To the best of our knowledge, this is the first report to demonstrate that RA reduces bone material strength by deteriorating the micro-arrangement of collagen/apatite bone matrix, leading to decreased fracture resistance. Our findings represent the significance of bone quality-based analysis for precise evaluation and subsequent therapy of the integrity and soundness of the bone in patients with RA.

1. Introduction

Rheumatoid arthritis (RA) is an autoimmune disease characterized by persistent synovitis and joint destruction [1], which affects approximately 0.5%–2.0% of the adult population and with 5–50 per 100,000 incidents/year in developed countries [2]. The innate immune system is closely linked to bone metabolism, and volumetric alterations in bone tissue related to destructive immunity have drawn the most attention for evaluating the severity of RA. The diagnosis, treatment, and monitoring of RA mainly involved plain radiography [3,4] or dual-energy X-ray absorptiometry (DXA) [5]. In particular, high-resolution computed tomography (CT), ultrasonography, and magnetic resonance imaging (MRI), which can reliably detect even small bone erosions [6], provided evidence for bone loss in both cortical and cancellous bone in RA [7]. Furthermore, recent studies using high-resolution peripheral quantitative CT (HR-pQCT) followed by micro-finite element analysis estimated the reduction in bone strength in RA patients [8,9].

With the development of biological drugs, including tumor necrosis factor (TNF) inhibitors, interleukin-6 (IL-6) receptor antibodies, and Janus kinase (JAK) inhibitors, treatment strategies for RA have been developed for decades [10]. However, establishment of the essential therapeutic resolution of RA to recover intact bone functions is still difficult. Bone functions are dominated by the organized micro-arrangement of bone matrix, and the degree of bone matrix orientation is recognized as a strong contributor to bone mechanical function [11–14]. Bone matrix micro-arrangement refers to the nanometer-scale

* Corresponding author at: Division of Materials and Manufacturing Science, Graduate School of Engineering, Osaka University, 2-1 Yamada-oka, Suita, Osaka 565-0871, Japan.
E-mail address: nakano@mat.eng.osaka-u.ac.jp (T. Nakano).
[1] These authors contributed equally to this work.

https://doi.org/10.1016/j.bone.2021.116261
Received 8 October 2021; Received in revised form 15 November 2021; Accepted 16 November 2021
Available online 23 November 2021

microstructure featured by preferential orientation of the main components of bone matrix: collagen and apatite crystallites. These components have anisotropic features owing to their unique atomic-scale structures [15,16]. Accumulating studies have highlighted that sole analysis of bone mineral density (BMD) is inadequate for understanding bone functions involving osteoporosis, cancer metastasis, or chronic kidney disease [13,17–23]. Under pathological conditions, cellular activities involved in organizing oriented bone matrix microstructure are disrupted by related biological molecular scenarios. More specifically, our recent findings have revealed that IL-6, one of the most abundant cytokines found in patients with active RA, disrupts osteoblast arrangement, the direct determinant of bone matrix organization [24]. These findings strongly indicate that inflammatory-related bone dysfunction in RA is associated with impaired bone structural microarrangement mediated by bone cellular functions.

This study demonstrated the impact of RA on matrix microarrangement, providing new insights into the determinant factor of bone fragility in the disease. Bone tissue strength, cortical size, and material properties, including volumetric BMD (vBMD) and bone matrix orientation, were analyzed in knee joints extracted from patients with RA and osteoarthritis (OA). Quantitative analysis of RA and OA contributions to bone strength was performed in subchondral bone at the periarticular proximal tibia. OA and RA are representative of the pathogenesis of arthritis and cause pain and joint damage. However, the underlying causes for these diseases are completely different; OA results from frequent cartilage breakdown due to daily wear and concentration of mechanical stress on the subchondral bone, whereas RA is an autoimmune disease. By selecting a bone portion (intercondylar eminence) wherein the effects of mechanical stress are negligibly small, we can study the effects of RA on bone matrix microstructure and mechanical function.

2. Materials and methods

2.1. Study design

Periarticular proximal tibiae were obtained from seven Japanese patients with RA and four Japanese patients with OA who underwent knee osteotomy at the Department of Orthopedic Surgery, National Hospital Organization Kyushu Medical Center. RA patients met the 1987 American College of Rheumatology (ACR) and/or 2010 ACR/European League Against Rheumatism classification criteria, and OA patients were able to exclude RA and had findings such as joint space narrowing and osteosclerosis on radiography. Larsen grading [25] for each joint was performed using radiography. Patient characteristics are shown in Table 1. The age of donors was significantly lower in RA (60 ± 12 years) than in OA (74 ± 3 years). Fig. 1A shows the representative bones from patients with RA and OA. There were findings of valgus knee deformity [26] in most of the bones in RA, and articular cartilage was lost at the lateral plateau. This study mainly focused on two parts of the bone according to the conditions of in vivo stress: the lateral plateau where joint contact pressures are locally applied [27], and the intercondylar eminence where less stresses are applied [28]. The lateral plateau and intercondylar eminence in patients with OA were described as the control group since loss of articular cartilage was noted in the medial plateau as often as it appeared in patients with OA. Despite the importance of intercondylar eminence in bone-governing knee functions [29], the medial condyles are also considered important regions for load bearing. Although the present study focused on the loading-independent alteration of bone micro-arrangement, the additional analysis of the medial condyles in RA is imperative and would be a near-future challenge. Bone specimens were immersed in neutral buffered formalin fixative immediately after extraction, replaced with 70% ethanol, and preserved until the experiments. The specimens were cut into approximately 1 mm-thick disks along the sagittal plane, as illustrated by the black lines in Fig. 1A. The bone properties were analyzed in the positions represented by the yellow and white stars (Fig. 1A). We defined the bone plane direction along the bone surface in the sagittal section as “parallel” and their normal directions as “vertical.” This study was approved by the Osaka University Committee for Ethical Guidelines on Research on Medical Systems Targeting People (approval number: R23), the Ethical Review Committee of Chugai Pharmaceutical Co. Ltd. (approval number: C119), and the Institutional Review Board of the National Hospital Organization Kyushu Medical Center (approval number: 17C174). All the study procedures were compliant with the Helsinki Declaration.

2.2. Biomechanical test

The articular cartilage attached to the subchondral bone was removed, and the bone specimen was naturally dried prior to the extrusion test. Extrusion tests [30] were performed on the subchondral bone surface, which showed a flattened smooth surface, adequate for homogeneous extrusion analysis on the axis vertical to the bone surface at a load rate of 1 mm/min. This was done using an Instron-type testing machine equipped with a prepared stainless extrusion rod (1.57 mm in diameter) and stainless steel. Tests were performed at room temperature and humidity. From the obtained load-displacement curve, the parameters of maximum load, stiffness, energy to failure, and maximum stress were used as indices of bone tissue strength. The maximum bone stress along the bone surface, which is the size-independent bone material strength, was calculated as the ratio of maximum load capacity to the contact area between the subchondral cortex and perimeter of the extrusion rod ($1.57\pi \times$ cortical thickness [mm^2]). The cortical thickness of the subchondral bone was determined as follows: micro-CT (μ-CT) at 50 kV and 85 μA to produce bone images with a spatial resolution of 30 μm and binarization of the images, as described previously [31]. The thickness was quantitatively measured using the TRI/3D-BON software (Ratoc System Engineering, Japan).

Table 1
Characteristics of patients.

No.	Group	Sex	Age [years]	Side	Duration of RA disease [years]	Medication history of anti-rheumatic drugs	Medication history of anti-osteoporotic drugs	Larsen grade
1	OA	F	72	R	0	No	No	–
2		F	72	L	0	No	No	–
3		F	79	L	0	No	No	–
4		M	73	R	0	No	Yes	–
5	RA	F	51	R	10	Yes	No	III
6		F	57	L	7	Yes	No	III
7		F	61	R	26	Yes	No	II
8		F	61	L	26	Yes	No	II
9		F	62	R	30	Yes	No	IV
10		M	46	R	33	Yes	No	III
11		M	85	R	6	No	Yes	IV

OA = osteoarthritis, RA = rheumatoid arthritis, F = female, M = male, R = right foot, L = left foot.

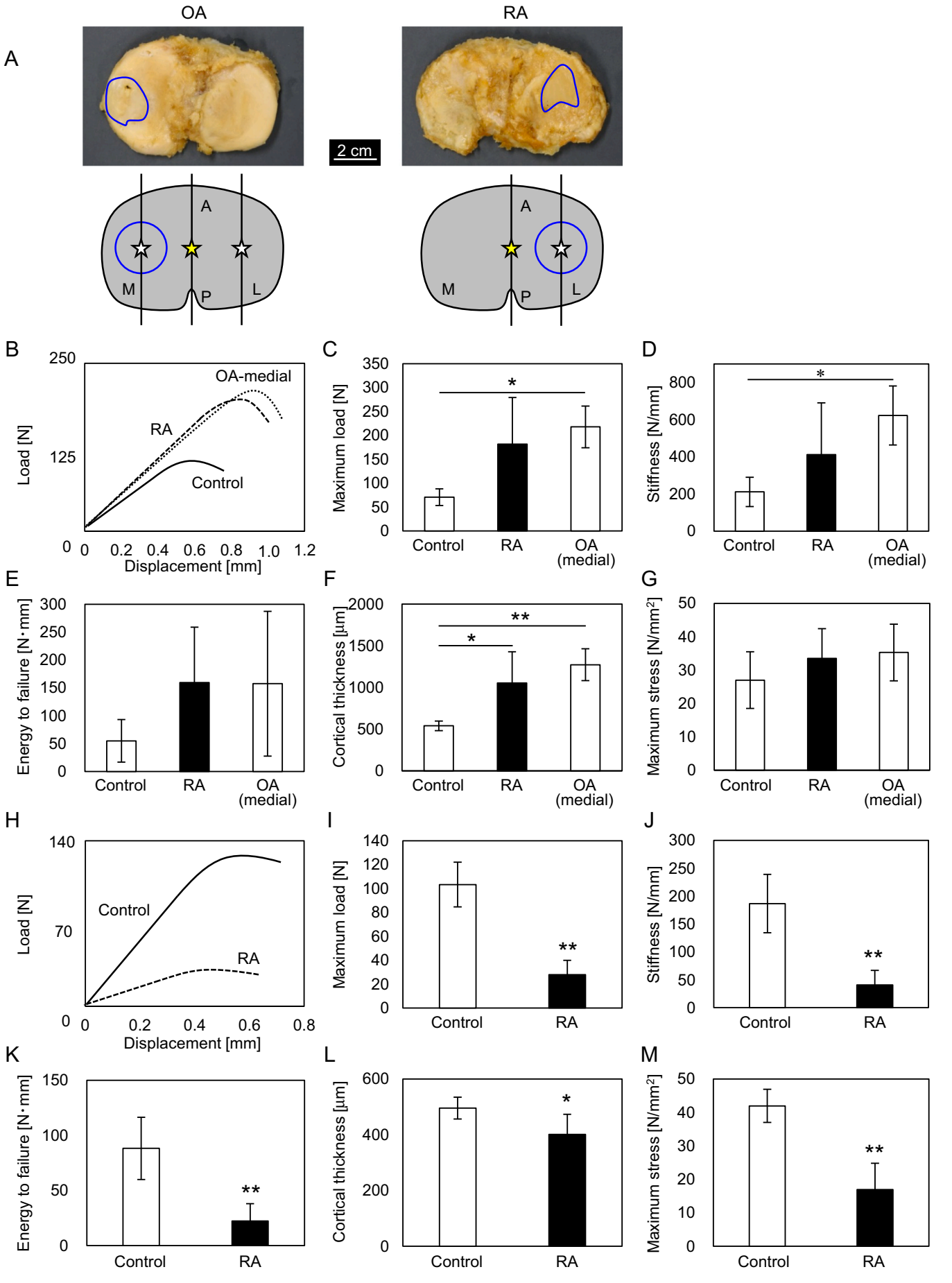

(caption on next page)

Fig. 1. Biomechanical properties of subchondral cortical bone of periarticular proximal tibiae. (A) Representative specimens of right periarticular proximal tibiae in patients with osteoarthritis (OA) and rheumatoid arthritis (RA). The upper images show bone appearance from the top view and the lower ones represent their schematic illustration. Bone areas surrounded by blue lines indicate bared bone without articular cartilage. OA bones lost articular cartilage at the medial plateau, whereas most of RA bones lost it at the lateral plateau. White (lateral and/or medial plateaus) and yellow (intercondylar eminence) stars indicate the analysis points in this study. A: anterior; P: posterior; M: medial; L: lateral. Load-displacement curve, maximum load, stiffness, and energy to failure are represented as bone tissue strength, cortical thickness, maximum stress as bone material strength of (B-G) lateral and/or medial plateaus, and (H-M) intercondylar eminence of proximal tibia, respectively. The medial part in OA, lateral part in OA, and lateral part in RA are represented as OA-medial, Control, and RA, respectively in (B-E). Intercondylar eminence in OA and RA are represented as Control and RA, respectively, in (H-M). **: $p < 0.01$ between Control and RA; *: $p < 0.05$ between Control and RA. OA: osteoarthritis; RA: rheumatoid arthritis. (For interpretation of the references to color in this figure legend, the reader is referred to the web version of this article.)

2.3. vBMD measurement by peripheral quantitative CT (pQCT)

The vBMD of the subchondral cortex was measured using a pQCT apparatus (XCT Research SA+; Stratec Medizintechnik GmbH, Birkenfeld, Germany). Bone specimens were scanned at a resolution of 70 × 70 × 260 μm^3. Cortical bone is generally defined above a threshold value of 690 mg/cm^3 [30]; therefore, the region of the subchondral cortex was determined by a vBMD value of ≥690 mg/cm^3 and bone shape.

2.4. Measurement of the preferential orientation of apatite c-axis by microbeam X-ray diffractometer (μ-XRD) system

The spatial distribution of the crystallographic *c*-axis orientation of apatite crystallites was analyzed using a μ-XRD system (R-Axis BQ; Rigaku, Tokyo, Japan) with a transmission-type optical system and imaging plate (storage phosphors; Fuji Film, Tokyo, Japan) placed behind the specimen. This study referred to the conditions for μ-XRD described in previous literature [11] and added minor modifications. The incident X-ray beam was collimated into a 300 μm (for subchondral cortical bone) or 800 μm (for cancellous bone) circular spot and projected vertically onto the sagittal plane of the bone specimen to analyze the in-plane orientation of the apatite *c*-axis. The minimum thickness of the subchondral cortex analyzed in this study was approximately 300 μm; therefore, X-ray diffraction data from the region 300 μm directly below the proximal surface of the subchondral bone was obtained when analyzing the cortical bone. The diffracted beam was collected for 600 s (for subchondral cortical bone) or 300 s (for cancellous bone) to obtain adequate diffraction intensity with a high signal/noise ratio.

The (002) crystal plane is generally used as a representative for analyzing the apatite *c*-axis, and the (310) plane is orthogonal to the (002) plane. From the acquired diffraction data, two diffraction peaks of apatite (002) and (310) were integrated for each azimuthal angle (β) at 1° increments. The intensity distributions of either (002) or (310) as a function of β for the diffraction intensities were individually fitted according to the literature [32,33]. The degree of crystallographic orientation of apatite *c*-axis was calculated for each β as the ratio of (002) intensity to (310) intensity ($I_{002}(\beta)/I_{310}(\beta)$) (Fig. 3A). This resulted in a two-dimensional apatite *c*-axis orientation as a function of β along the plane vertical to the incident X-ray beam, which is shown as a radar diagram. In this apparatus, randomly oriented hydroxyapatite powder had a value of 0.6. The data, including the value of $I_{002}(\beta)/I_{310}(\beta)$ in the axis parallel or vertical to the bone surface, maximum value of $I_{002}(\beta)/I_{310}(\beta)$, and the deviation angle from the axis parallel to the bone surface were quantified. Measurements were performed at three points for cortical bone and nine points for cancellous bone at a certain interval in each bone specimen, as shown in Fig. 3B. The data were averaged, and the σ_{Angle}, which is the standard deviation of the preferential orientation angle in each bone specimen, was analyzed to evaluate the directional uniformity of the apatite *c*-axis orientation.

2.5. Measurement of collagen orientation by birefringence method

To evaluate the spatial distribution of preferential collagen orientation, bone sections were observed using a two-dimensional birefringence measurement system (WPA-micro, Photonic Lattice, Miyagi, Japan) attached to an upright microscope (BX60; Olympus, Tokyo, Japan). Birefringence analysis was performed using WPA-VIEW software (version 2.4.2.9; Photonic Lattice), as previously described [13]. For quantitative comparison of collagen orientation, the orientation order parameter f_θ was calculated based on the orientation angle distribution of collagen against the bone surface plane [34]. The birefringence images were obtained at 12 points in an area of 530 μm × 400 μm for each sample. The measured areas correspond to the portion of apatite orientation analysis. f_θ takes a value ranging from −1 (collagen perfectly aligned perpendicular to the bone surface of subchondral cortical bone) to 1 (collagen perfectly aligned parallel to the bone surface of subchondral cortical bone). Non-decalcified bone of 5-6 μm thickness and with Villanueva bone stain were analyzed in this study. Fluorescence observations of the bone sections were performed to evaluate the osteocyte conditions. Images were obtained using a fluorescence microscope (BZ-510; Keyence, Osaka, Japan).

2.6. Statistical analysis

The data were acquired from seven bones with RA and four bones with OA, and the data are shown as mean ± standard deviation. Statistical significance between the two groups was tested using the nonparametric Mann-Whitney *U* test. One-way analysis of variance was conducted for comparing the three groups, followed by Tukey's multiple comparison tests. Single and multiple regression analyses were performed to determine the explanatory variables of bone tissue strength. To detect multicollinearity prior to multiple regression analyses, tolerance and variance inflation factors (VIFs) were calculated. Statistical significance was set at a *p*-value of <0.05. SPSS version 14.0 J (SPSS Japan Inc., Japan) for Microsoft Windows was used for the statistical analyses.

3. Results

3.1. Bone mechanical properties of subchondral bone

An extrusion test was performed to determine the strength of the subchondral bone (Fig. 1). In the lateral plateau, the RA group showed greater maximum load capacity (+156%) than the control group (Fig. 1B, C) due to thickening of the subchondral bone (Fig. 1F).

However, bone material strength in this bone region was statistically comparable between the experimental groups (Fig. 1G). These characteristics of the lateral plateau in the RA group resembled those of the bare bone without the articular cartilage at the medial plateau of the OA bone (Fig. 1B-F). In the intercondylar eminence, the behaviors of the load-displacement curves were quite different between the RA and control groups (Fig. 1H). The RA group showed significantly reduced maximum load capacity compared with the control group (Fig. 1I), indicating that fracture tolerance was lower (−73%) in the RA group. Cortical thickness resulting from bone erosion was significantly lower (−19%) in the RA group than in the control group (Fig. 1L). Furthermore, size-independent bone material strength was significantly lower (−60%) in the RA group (Fig. 1M). These results suggest that deteriorated bone material strength strongly influences the degradation of bone tissue strength. Therefore, subsequent analyses focused on the material properties in the intercondylar eminence of the proximal tibia.

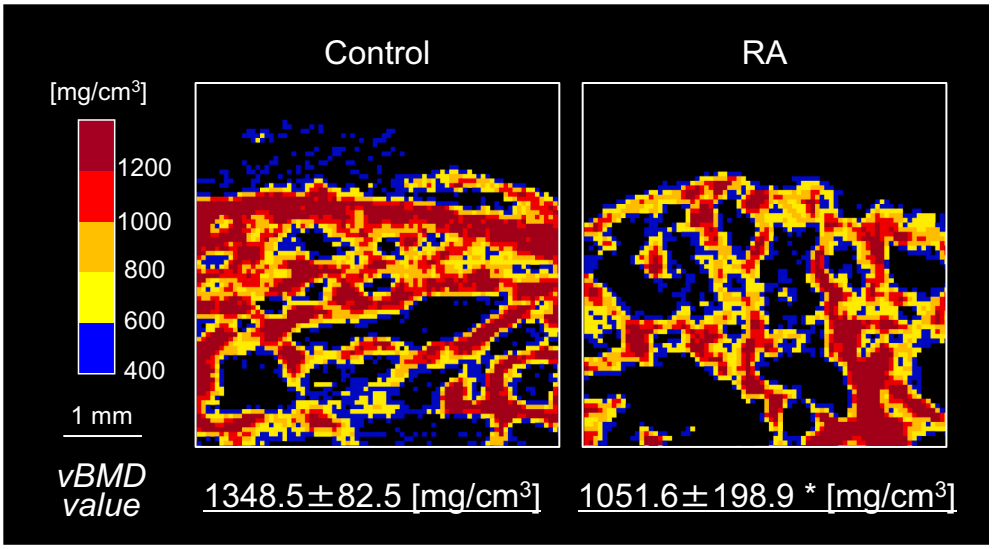

Fig. 2. Volumetric bone mineral density (vBMD) measured in subchondral bone of periarticular proximal tibia. The averaged vBMD value is indicated below each color map. Color indicates the value of vBMD in each pixel. *: $p < 0.05$. RA: rheumatoid arthritis. (For interpretation of the references to color in this figure legend, the reader is referred to the web version of this article.)

3.2. vBMD of subchondral bone

Bone material strength is determined by material properties, namely, the density and quality of the bone matrix. To determine bone matrix density, vBMD was analyzed in the subchondral cortical bone (Fig. 2). The RA bone showed a significantly lower vBMD value (−22%) compared with the control bone. Together with the results in Fig. 1H, it was confirmed that RA decreased bone mass in the subchondral bone.

3.3. Apatite c-axis orientation of subchondral bone and cancellous bone

The spatial distribution of apatite *c*-axis orientation was analyzed along the sagittal plane in the subchondral cortex and cancellous bones (Fig. 3). In the control group, apatite *c*-axis uniformly aligned parallel to the bone surface in the subchondral cortex ($\sigma_{Angle} = 3.7 \pm 2.3$), as observed in the radar diagram (Fig. 3B). The degree of preferential apatite *c*-axis orientation along the parallel axis was approximately 2.7 times higher than that along its vertical axis, showing a strong anisotropic alignment in the control group (Fig. 3C). In contrast, the subchondral cortex in the RA group showed heterogeneous alignment of apatite *c*-axis ($\sigma_{Angle} = 21.8 \pm 8.9$) and significantly reduced the maximum value of the apatite *c*-axis orientation degree compared with the control group (Fig. 3C). Therefore, the RA group decreased the apatite *c*-axis orientation along the parallel axis (−45%), indicating a failure of anisotropic alignment of apatite crystallites (Fig. 3B, C). Furthermore, the RA group disturbed the alignment in cancellous bone ($\sigma_{Angle} = 26.4 \pm 4.0$) compared with control bone ($\sigma_{Angle} = 20.7 \pm 5.3$), and significantly decreased preferential orientation of apatite *c*-axis along the bone surface axis, as shown in Fig. 3B and D.

3.4. Collagen molecule orientation of subchondral bone and cancellous bone

The spatial distribution of collagen orientation was analyzed in the corresponding region where other analyses were conducted (Fig. 4). In the control group, collagen preferentially aligned parallel to the bone surface in the sagittal plane, whereas the RA group showed more homogenous collagen directionality in both the subchondral bone and cancellous bone, as indicated on the orientation color map (Fig. 4A). Because collagen is a positive birefringent material, the direction of the slow axis corresponds to the direction along the length of collagen fibrils [35]. The average orientation of the slow axis (φ) for each pixel was analyzed. The two-dimensional distribution of φ is indicated by colors. The degree of collagen orientation parallel to the bone surface was significantly lower in the RA group than in the control group (Fig. 4B). The change in collagen orientation significantly correlates with the degree of preferential apatite *c*-axis orientation parallel to the bone surface in both the subchondral cortex ($R^2 = 0.72$, $p = 8.7 \times 10^{-4}$) and cancellous bone ($R^2 = 0.58$, $p = 6.2 \times 10^{-3}$). These results demonstrate that RA disturbs the alignment of collagen/apatite crystallites. Furthermore, osteocyte lacunae aligned approximately parallel along the bone surface axis, and the canaliculi tightly connected with each other in the control group, whereas neither of these findings were observed in the RA group (Fig. 4C).

3.5. Contributions of vBMD and bone matrix orientation to material strength of subchondral bone

To determine the main determinant of reduced bone material strength in RA, single and multiple regression analyses were performed. Note that, between the preferential orientation of collagen and apatite *c*-axis, only the latter was used for regression analyses. This is because the long axis of collagen fibrils and the apatite *c*-axis intrinsically have an approximately parallel relationship based on the epitaxial growth of apatite crystals on the collagen template in the *in vivo* self-assembly process [36]. To prevent the effects of multicollinearity in multiple regression analysis, it is essential to use parameters that are independent of each other. In this study, multicollinearity was not found between vBMD and the degree of apatite *c*-axis orientation (*tolerance* = 0.61 > 0.1, *VIF* = 1.64 < 10); thus, these parameters were used as independent explanatory variables for multiple regression analysis of maximum stress capacity. From the analysis, the maximum stress capacity of bone was significantly and positively correlated with both vBMD ($R^2 = 0.65$, $p = 2.8 \times 10^{-3}$) and the degree of apatite *c*-axis orientation along the subchondral bone ($R^2 = 0.70$, $p = 1.4 \times 10^{-3}$) (Fig. 5). Multiple regression analysis showed that changes in these variables significantly contributed to the decrease in maximum stress capacity of bone in RA. The degree of apatite *c*-axis orientation significantly contributed to mechanical function as well as vBMD, as represented by the value of β (Table 2).

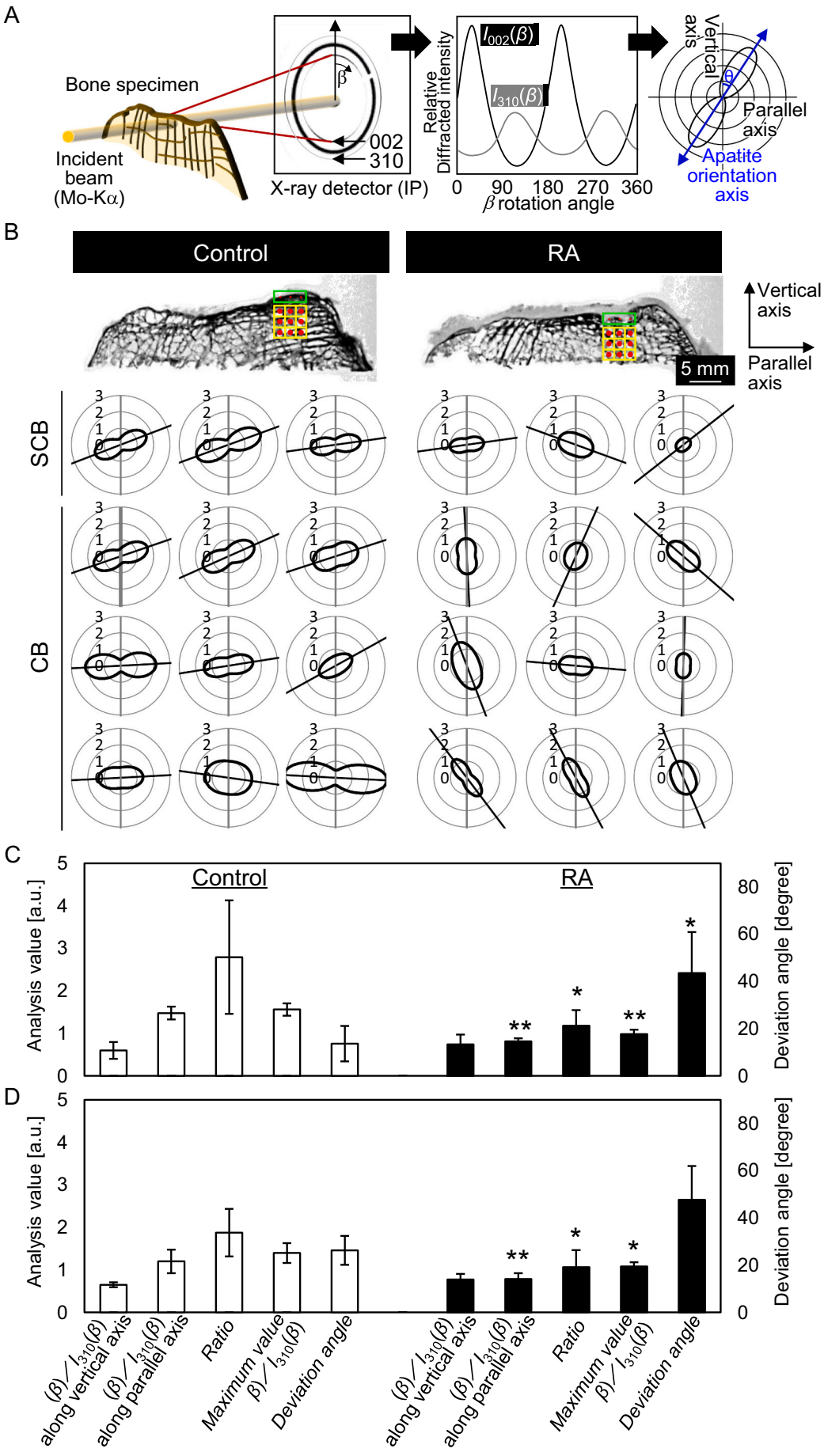

(caption on next page)

Fig. 3. Preferential orientation of apatite *c*-axis measured in subchondral bone and cancellous bone of the periarticular proximal tibia. (A) A schematic illustration of measurement of apatite *c*-axis orientation by microbeam X-ray diffraction and the following analysis for intensity ratio of (002)/(310) along β rotation. θ corresponds to the major axis angle with a maximum intensity of (002)/(310). (B) Radar diagrams analyzed subchondral bone and cancellous bone, showing the degree of apatite *c*-axis orientation ($I_{002}(\beta)/I_{310}(\beta)$) along β rotation. The analysis points in radiographic images are represented by red dots. The size of the dots coincides with the diameter of the X-ray collimator in this scale. RA: rheumatoid arthritis; SCB: subchondral bone; CB: cancellous bone. Quantitative data of spatial distribution of apatite *c*-axis orientation include (i) degree of apatite *c*-axis orientation along the axis vertical to bone surface, (ii) degree of apatite *c*-axis orientation along the axis parallel to bone surface, (iii) ratio of degree of apatite *c*-axis orientation along parallel axis to that along vertical axis, (iv) maximum value of degree of apatite *c*-axis orientation, and (v) deviation angle of preferential orientation from parallel axis in (C) the subchondral bone and (D) cancellous bone. Left and right ordinates express the value of (i)-(iv) and (v), respectively. **: $p < 0.01$; *: $p < 0.05$. a.u.: arbitrary unit.

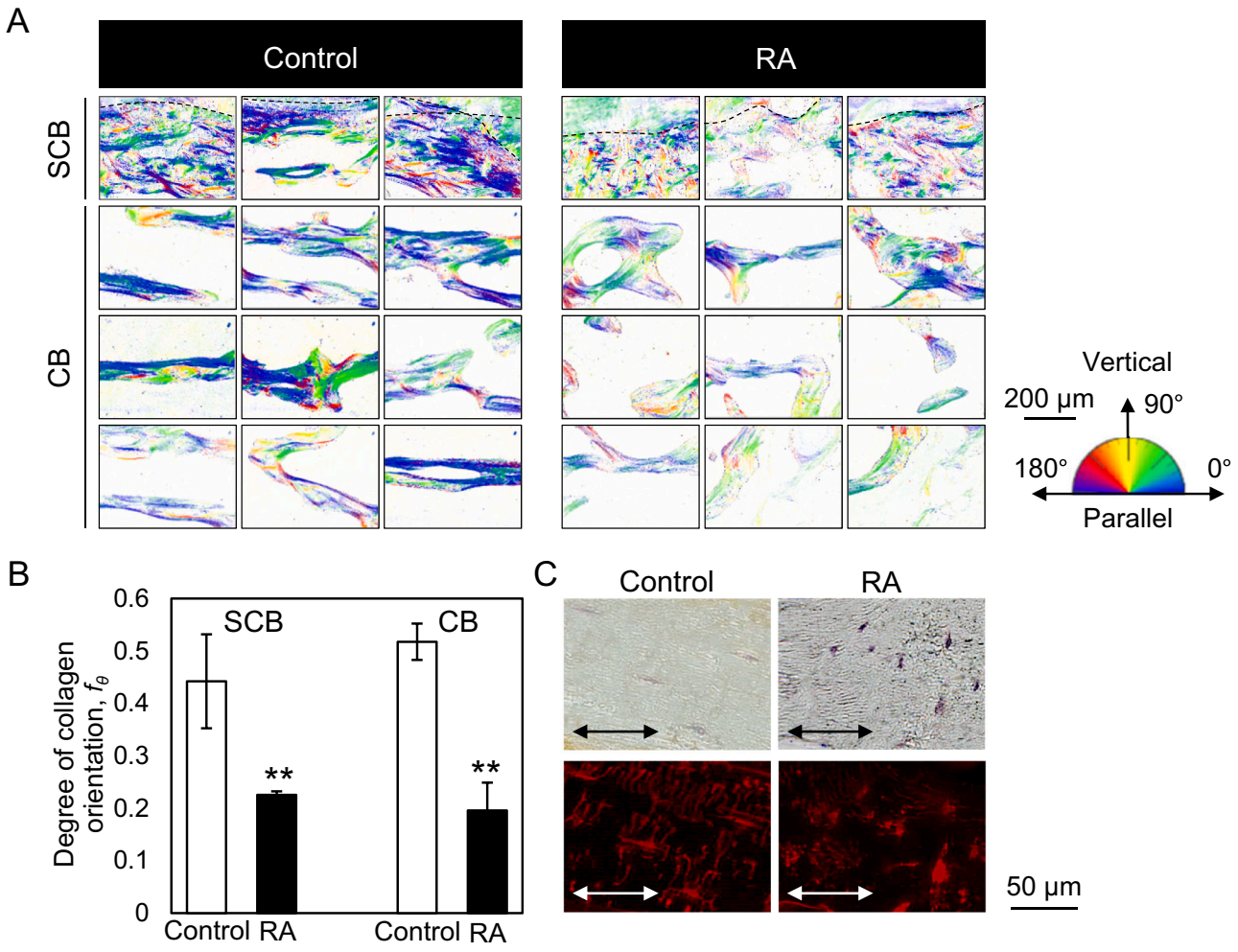

Fig. 4. Preferential orientation of collagen measured in subchondral bone and cancellous bone of the periarticular proximal tibia. (A) Color map corresponds to the slow axis of birefringence, which corresponds to the direction along the length of collagen fibrils and (B) quantitative degree of the collagen orientation parallel to the bone surface. (C) Morphological observation of osteocytes by bright field images and fluorescent images are shown. Bidirectional arrows indicate the direction parallel to the bone surface. **: $p < 0.01$. RA: rheumatoid arthritis; SCB: subchondral bone; CB: cancellous bone. (For interpretation of the references to color in this figure legend, the reader is referred to the web version of this article.)

4. Discussion

A long history of RA research has exclusively focused on the elevated bone resorption pathology in the patients suffering from the disease; alteration of bone quality, especially the microstructural abnormality in RA has been overlooked for decades. The important finding of this study is that the deterioration of bone matrix orientation in RA is a key contributor to loss of bone material strength, resulting in severe bone fragility in the knee joint. Notably, a significant difference was found in age between RA donors and control (OA) donors. The changes observed in the RA bone cannot be attributed to aging because the deterioration of micro-arrangement of bone material and loss of strength in younger RA bones are contradictory to the general changes associated with aging.

RA generates heterogeneous physical and biological environments depending on the anatomical portion. The intercondylar area is exposed to biologically induced inflammation conditions without any specific in vivo stress [27]. In contrast, the medial and lateral tibial plateaus are subjected to further stresses and joint contact pressures ranging from 10 to 20 MPa [26]. Therefore, bone mechanical properties in relation to the anisotropic microstructure in RA bone vary depending on the focused position. The bone material strength in the intercondylar eminence in RA prominently exhibited a lower material strength value via bone matrix degradation, whereas the lateral plateau showed increased bone strength beyond the normal value. In the weight-bearing lateral plateau of the proximal tibia in RA, articular cartilage covering the bone surface and providing a cushioning effect for load-bearing bone [37] was lost

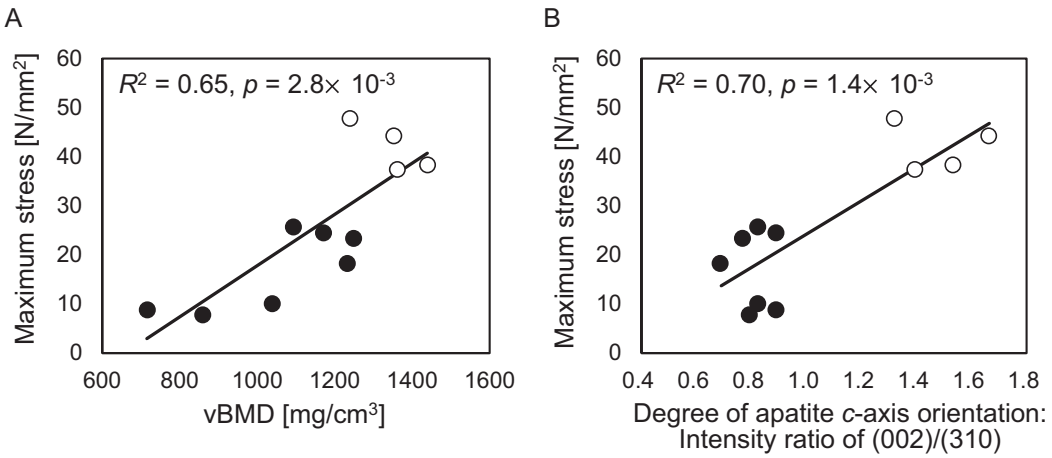

Fig. 5. Relationship between bone material properties and bone material strength. (A) vBMD vs. maximum stress capacity of bone. (B) Degree of apatite c-axis orientation vs. maximum stress capacity of bone. White and black circles indicate the measured value of control and rheumatoid arthritis (RA) groups, respectively. vBMD: volumetric bone mineral density.

due to continued synovial inflammation coupled with abnormal biomechanics in the knee joint [1]. A load greater than normal imposed a morphological macroscopic structural change (subchondral sclerosis) on bone, which possibly counteracted the effects of RA-induced inflammation on bone characteristics. Therefore, the bone region developed OA-like changes in appearance [38,39] and mechanical functions of bone tissue. Previous studies have also provided evidence for the development of bone protrusions [40] and subchondral sclerosis [41], resembling that noted in OA in patients with RA. In addition, the present study clearly indicates the development of secondary OA in the RA-bearing bone, representing a significantly high degree of bone matrix alignment along the normal direction of the subchondral surface, consistent with the findings of a previous report [42].

Apart from the OA-like alteration in the tibial plateau of RA bone in relation to the inflammatory-derived mechanical environment, the intercondylar region experiences the biological effects of a dysregulated immune system. The results suggest that RA-induced inflammation deteriorates the collagen/apatite alignment in the subchondral region, generating weakened bone independent of mechanical effects. The micro-arrangement of collagen/apatite in the bone matrix is determined by various environmental factors, including in vivo stress distribution [11,32,43] and biological factors such as bone disorders [13,19–23,44,45]. In this study, a disordered arrangement of the osteocyte lacunae-canaliculi network and a less-aligned bone matrix orientation were observed in the subchondral region of the RA-bearing bone. This indicated possible involvement of osteocyte dysfunction in inflammation-induced bone matrix disarrangement and that osteocyte activity related to their network architecture is associated with bone matrix alignment. The quantitative analysis of the direction and connectivity of osteocytes is imperative for the characterization of RA bone, which will be investigated in the future. A recent study demonstrated the mirroring of organized osteocyte alignment and bone matrix micro-arrangement [21] and stated the impaired osteocyte network can trigger a disorganized microstructure in diseased bone [23]. The abnormal osteocyte network arrangement in RA-bearing bone possibly contributes to the disarrangement of collagen/apatite. Considering the possibility of sustained cell alignment during osteoblast–osteocyte transformation, disorganized osteocytes may be derived from impaired osteoblast alignment [46].

It is becoming increasingly evident that pro-inflammatory cytokines, including TNF-α, IL-6, and IL-1β, influence Wnt signaling by regulating sclerostin expression in osteocytes, further contributing to increased bone resorption and decreased bone formation in RA [3]. Furthermore, inflammatory signals induce osteocyte apoptosis, which mediates bone loss in inflammatory diseases [47]. Among inflammatory-related signals, IL-6 plays a central role in the pathogenesis of RA; tocilizumab, an anti-IL-6 receptor antibody that inhibits the downstream JAK/STAT pathway, has been approved for the treatment of RA [48]. The current finding of IL-6 as a regulatory factor for osteoblast arrangement [24] indicates that inflammatory-related cytokines disrupt the organized cytoskeletal arrangement of cells and further induce disorganized microstructure of the bone matrix. Moreover, the latest research revealed that patients diagnosed with cytokine release syndrome, including sudden acute respiratory syndrome coronavirus 2 (SARS-CoV-2) infection (COVID-19), show elevated levels of IL-6 [49], indicating that SARS-CoV-2 infection possibly induces the disordered arrangement of bone tissue via the IL-6 signaling pathway.

In clinical settings, radiographic evaluation involving Larsen grading [25], Sharp grading [50], and the modified grading method [51,52] have been widely used to diagnose the severity of RA. Larsen grading is a prominent factor for detecting RA incidence. However, the corresponding grade in this study did not accurately reflect bone characteristics and functions, with the following correlation relationship: bone tissue strength ($R^2 = 1.6 \times 10^{-2}, p = 0.79$), bone material strength ($R^2 = 1.8 \times 10^{-2}, p = 0.77$), vBMD ($R^2 = 7.1 \times 10^{-3}, p = 0.86$), apatite c-axis orientation ($R^2 = 9.2 \times 10^{-2}, p = 0.51$), and collagen orientation ($R^2 = 1.4 \times 10^{-3}$, $p = 0.93$). The present findings indicate that bone dysfunction in RA cannot be estimated without assessing the microstructure of diseased bone as a bone quality index. Alternative noninvasive or less invasive methods to detect bone micro-arrangement are imperative and are expected to be developed. One possible candidate for noninvasive analysis is the use of speed of ultrasound (SOS), which is already used in clinical settings for monitoring osteoporotic bone changes. SOS reportedly reflects the degree of apatite orientation [53]. However, the SOS information also includes the effects of porosity or compositional alteration, and it would be desirable to determine diagnosis considering these effects on SOS measurement. In addition, as one of the other bone quality indices, collagen cross-linking is a definite contributor to bone strength [54,55]. Oxidative stress contributes to RA pathogenesis, and collagen oxidation may be related to the degraded

Table 2
Relative contributions of vBMD and apatite c-axis orientation to bone material strength determined by multiple regression analysis.

vBMD		Apatite c-axis orientation	
β	p	β	p
0.46	3.8×10^{-2}	0.52	1.9×10^{-2}

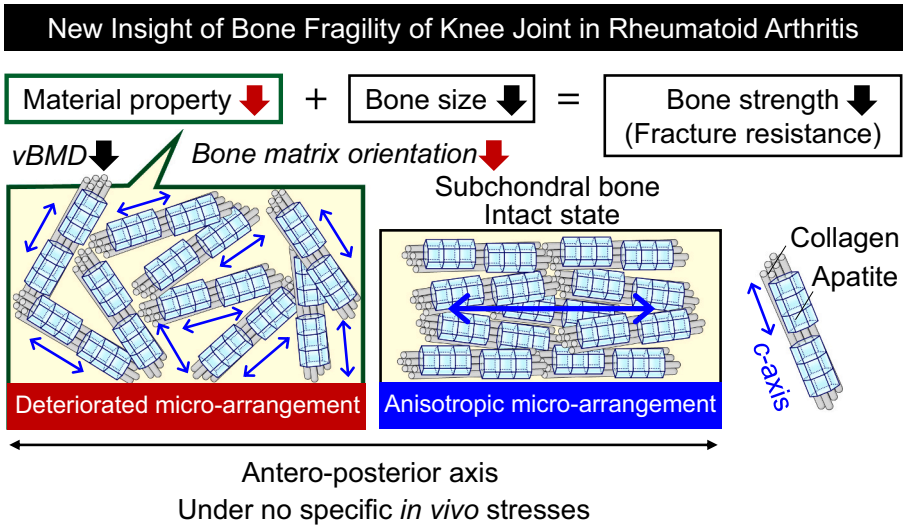

Fig. 6. Schematic illustration of the cause of bone fragility of knee joint in rheumatoid arthritis (RA). Bone fragility in RA is strongly caused by the deterioration of bone material property via degradation of collagen and apatite crystallite micro-arrangement. vBMD: volumetric bone mineral density.

bone strength in patients with RA [56]. Indeed, collagen cross-linking has been increasingly recognized to be related to bone matrix micro-arrangement [57]. Clarifying this issue would be a challenge in future investigations.

In conclusion, the degradation of bone matrix orientation and bone quality index are determining factors that increase the risk of fracture in RA-bearing bone as well as vBMD (Fig. 6). RA reduces bone material strength by the deterioration of bone matrix micro-arrangement, resulting in impaired bone function. Increasing evidence indicates that inflammatory-related cytokines are involved in the disorganization of bone matrix microarchitecture in RA. The findings obtained in this study provide novel therapeutic targets for impaired microstructural construction in RA-bearing bone and contributing to the management of fracture resistance. A potential therapeutic strategy for the recovery of bone matrix micro-arrangement is to introduce an anisotropic guiding structure as a bone ingrowth scaffold. Implantation-guided cell alignment is an important initiator for the formation of a collagen/apatite micro-arrangement. Control of bone tissue anisotropy has been achieved using the grooved surface of hip implants [33] and open-spaced spine devices [31]. In addition, several biomarkers for bone anisotropy are increasingly recognized as important therapeutic targets for bone health [58].

CRediT authorship contribution statement

Ryosuke Ozasa: Data curation, Formal analysis, Investigation, Methodology, Visualization, Writing – original draft. **Aira Matsugaki:** Data curation, Formal analysis, Investigation, Methodology, Visualization, Writing – original draft. **Takuya Ishimoto:** Data curation, Formal analysis, Investigation, Methodology, Visualization, Writing – original draft. **Satoshi Kamura:** Validation, Supervision. **Hiroto Yoshida:** Investigation. **Mayu Magi:** Investigation. **Yoshihiro Matsumoto:** Investigation, Validation. **Koji Sakuraba:** Investigation. **Kenjiro Fujimura:** Investigation. **Hisaaki Miyahara:** Investigation. **Takayoshi Nakano:** Conceptualization, Methodology, Validation, Writing – review & editing, Supervision, Project administration.

Declaration of competing interest

RO, AM, TI, KS, KF, and HM have no conflict of interest. HY, MM, and YM are employees of Chugai Pharmaceutical Co., Ltd. SK and TN have received research funding from Chugai Pharmaceutical Co., Ltd.

Acknowledgments

This work was supported by Grants-in-Aid for Scientific Research from the Japan Society for the Promotion of Science (JSPS) [grant numbers JP18H05254] and research fund from Chugai Pharmaceutical Co., Ltd.

Data availability

The raw and processed data required to reproduce these findings are available at Mendeley Data, V1, 10.17632/d7czw3bczy.1.

References

[1] I.B. McInnes, G. Schett, Cytokines in the pathogenesis of rheumatoid arthritis, Nat. Rev. Immunol. 7 (2007) 429–442.
[2] D.L. Scott, F. Wolfe, T.W.J. Huizinga, Rheumatoid arthritis, Lancet 376 (2010) 1094–1108.
[3] G. Schett, E. Gravallese, Bone erosion in rheumatoid arthritis: mechanisms, diagnosis and treatment, Nat. Rev. Rheumatol. 8 (2012) 656–664.
[4] K.P. Machold, T.A. Stamm, V.P.K. Nell, S. Pflugbeil, D. Aletaha, G. Steiner, M. Uffmann, et al., Very recent onset rheumatoid arthritis: clinical and serological patient characteristics associated with radiographic progression over the first years of disease, Rheumatology 46 (2007) 342–349.
[5] S. Bobo Tanner, C.F. Moore Jr., A review of the use of dual-energy X-ray absorptiometry (DXA) in rheumatology, Open Access Rheumatol. 4 (2012) 99–107.
[6] U.M. Døhn, B. Ejbjerg, A. Boonen, M.L. Hetland, M.S. Hansen, L.S. Knudsen, et al., No overall progression and occasional repair of erosions despite persistent inflammation in adalimumab-treated rheumatoid arthritis patients: results from a longitudinal comparative MRI, ultrasonography, CT and radiography study, Ann. Rheum. Dis. 70 (2011) 252–258.
[7] R. Kocijan, S. Finzel, M. Englbrecht, K. Engelke, J. Rech, G. Schett, Differences in bone structure between rheumatoid arthritis and psoriatic arthritis patients relative to autoantibody positivity, Ann. Rheum. Dis. 73 (2014) 2022–2028.
[8] N.N. Haroon, E. Szabo, J.M. Raboud, H. Mcdonald-Blumer, L. Fung, R.G. Josse, et al., Alterations of bone mineral density, bone microarchitecture and strength in patients with ankylosing spondylitis: a cross-sectional study using high-resolution peripheral quantitative computerized tomography and finite element analysis, Arthritis Res. Ther. 17 (2015) 1–9.
[9] F. Stemmler, D. Simon, A.M. Liphardt, M. Englbrecht, J. Rech, A.J. Hueber, et al., Biomechanical properties of bone are impaired in patients with ACPA-positive rheumatoid arthritis and associated with the occurrence of fractures, Ann. Rheum. Dis. 77 (2018) 973–980.
[10] A.A. Drosos, E. Pelechas, P.V. Voulgari, Treatment strategies are more important than drugs in the management of rheumatoid arthritis, Clin. Rheumatol. 39 (2020) 1363–1368.
[11] T. Nakano, K. Kaibara, Y. Tabata, N. Nagata, S. Enomoto, E. Marukawa, et al., Unique alignment and texture of biological apatite crystallites in typical calcified tissues analyzed by microbeam x-ray diffractometer system, Bone 31 (2002) 479–487.
[12] T. Ishimoto, T. Nakano, Y. Umakoshi, M. Yamamoto, Y. Tabata, Degree of biological apatite c-axis orientation rather than bone mineral density controls

mechanical function in bone regenerated using recombinant bone morphogenetic protein-2, J. Bone Miner. Res. 28 (2013) 1170–1179.
[13] R. Ozasa, T. Ishimoto, S. Miyabe, J. Hashimoto, M. Hirao, H. Yoshikawa, et al., Osteoporosis changes collagen/apatite orientation and Young's modulus in vertebral cortical bone of rat, Calcif. Tissue Int. 104 (2019) 449–460.
[14] T. Moriishi, R. Ozasa, T. Ishimoto, T. Nakano, T. Hasegawa, T. Miyazaki, et al., Osteocalcin is necessary for the alignment of apatite crystallites, but not glucose metabolism, testosterone synthesis, or muscle mass, PLoS Genet. 16 (2020), e1008586.
[15] M.P.E. Wenger, L. Bozec, M.A. Horton, P. Mesquidaz, Mechanical properties of collagen fibrils, Biophys. J. 93 (2007) 1255–1263.
[16] B. Viswanath, R. Raghavan, U. Ramamurty, N. Ravishankar, Mechanical properties and anisotropy in hydroxyapatite single crystals, Scr. Mater. 57 (2007) 361–364.
[17] B.L. Riggs, L.J. Melton Iii, Bone turnover matters: the raloxifene treatment paradox of dramatic decreases in vertebral fractures without commensurate increases in bone density, J. Bone Miner. Res. 17 (2002) 11–14.
[18] P. Ammann, Bone strength and its determinants, Osteoporos. Int. 58 (2003) 403–407.
[19] T. Wakamatsu, Y. Iwasaki, S. Yamamoto, K. Matsuo, S. Goto, I. Narita, et al., Type-I angiotensin II receptor blockade reduces uremia-induced deterioration of bone material properties, J. Bone Miner. Res. 36 (2021) 67–79.
[20] A. Sekita, A. Matsugaki, T. Nakano, Disruption of collagen/apatite alignment impairs bone mechanical function in osteoblastic metastasis induced by prostate cancer, Bone 97 (2017) 83–93.
[21] T. Ishimoto, K. Kawahara, A. Matsugaki, H. Kamioka, T. Nakano, Quantitative evaluation of osteocyte morphology and bone anisotropic extracellular matrix in rat femur, Calcif. Tissue Int. 109 (2021) 434–444.
[22] M. Tanaka, A. Matsugaki, T. Ishimoto, T. Nakano, Evaluation of crystallographic orientation of biological apatite at vertebral cortical bone in ovariectomized cynomolgus monkey treated with minodronic acid and alendronate, J. Bone Miner. Metab. 34 (2016) 234–241.
[23] A. Sekita, A. Matsugaki, T. Ishimoto, T. Nakano, Synchronous disruption of anisotropic arrangement of the osteocyte network and collagen/apatite in melanoma bone metastasis, J. Struct. Biol. 197 (2017) 260–270.
[24] A. Matsugaki, S. Matsumoto, T. Nakano, A novel role of interleukin-6 as a regulatory factor of inflammation-associated deterioration in osteoblast arrangement, Int. J. Mol. Sci. 21 (2020) 6659.
[25] A. Larsen, K. Dale, M. Eek, Radiographic evaluation of rheumatoid arthritis and related conditions by standard reference films, Acta Radiol. Diagn. 18 (1977) 481–491.
[26] L. Sharma, J.S. Chmiel, O. Almagor, D. Felson, A. Guermazi, F. Roemer, et al., The role of varus and valgus alignment in the initial development of knee cartilage damage by MRI: the MOST study, Ann. Rheum. Dis. 72 (2013) 235–240.
[27] B.J. Fregly, Y. Bei, M.E. Sylvester, Experimental evaluation of an elastic foundation model to predict contact pressures in knee replacements, J. Biomech. 36 (2003) 1659–1668.
[28] L.L. Frazer, E.M. Santschi, K.J. Fischer, Impact of a void in the equine medial femoral condyle on bone stresses and peak contact pressures in a finite element model, Vet. Surg. 48 (2019) 237–246.
[29] C.N. Anderson, A.F. Anderson, Tibial eminence fractures, Clin. Sports Med. 30 (2011) 727–742.
[30] Z.G. Jia, W. Li, Z.R. Zhou, Mechanical characterization of stomach tissue under uniaxial tensile action, J. Biomech. 48 (2015) 651–658.
[31] T. Ishimoto, K. Yamada, H. Takahashi, M. Takahata, M. Ito, T. Hanawa, et al., Trabecular health of vertebrae based on anisotropy in trabecular architecture and collagen/apatite micro-arrangement after implantation of intervertebral fusion cages in the sheep spine, Bone 108 (2018) 25–33.
[32] T. Ishimoto, B. Sato, J.W. Lee, T. Nakano, Co-deteriorations of anisotropic extracellular matrix arrangement and intrinsic mechanical property in c-src deficient osteopetrotic mouse femur, Bone 103 (2017) 216–223.
[33] Y. Noyama, T. Nakano, T. Ishimoto, T. Sakai, H. Yoshikawa, Design and optimization of the oriented groove on the hip implant surface to promote bone microstructure integrity, Bone 52 (2013) 659–667.
[34] R. Ozasa, A. Matsugaki, Y. Isobe, T. Saku, H.S. Yun, T. Nakano, Construction of human induced pluripotent stem cell-derived oriented bone matrix microstructure by using in vitro engineered anisotropic culture model, J. Biomed. Mater. Res. A 106 (2018) 360–369.
[35] N.M. Kalyani, C.A. Ong, A.C. Lysaght, S.J. Haward, G.H. McKinley, K.M. Stankovic, Quantitative polarized light microscopy of unstained mammalian cochlear sections, J. Biomed. Opt. 18 (2013) 26021.
[36] W.J. Landis, K.J. Hodgens, M.J. Song, J. Arena, S. Kiyonaga, M. Marko, et al., Mineralization of collagen may occur on fibril surfaces: evidence from conventional and high-voltage electron microscopy and three-dimensional imaging, J. Struct. Biol. 117 (1996) 24–35.
[37] J.R. Matyas, L. Atley, M. Ionescu, D.R. Eyre, A.R. Poole, Analysis of cartilage biomarkers in the early phases of canine experimental osteoarthritis, Arthritis Rheumatol. 50 (2004) 543–552.
[38] Y. Wang, A.E. Wluka, J.P. Pelletier, J. Martel-Pelletier, F. Abram, C. Ding, et al., Meniscal extrusion predicts increases in subchondral bone marrow lesions and bone cysts and expansion of subchondral bone in osteoarthritic knees, Rheumatology 49 (2010) 997–1004.
[39] G. Li, J. Yin, J. Gao, N.J. Pavlos, C. Zhang, M.H. Zheng, Subchondral bone in osteoarthritis: insight into risk factors and microstructural changes, Arthritis Res. Ther. 15 (2013) 1–2.
[40] C.P. Figueiredo, D. Simon, M. Englbrecht, J. Haschka, A. Kleyer, S. Bayat, et al., Quantification and impact of secondary osteoarthritis in patients with anti–citrullinated protein antibody–positive rheumatoid arthritis, Arthritis Rheumatol. 68 (2016) 2114–2121.
[41] L. Solomon, Patterns of osteoarthritis of the hip, J. Bone Jt Surg. 58 (1976) 176–183.
[42] J.W. Lee, A. Kobayashi, T. Nakano, Crystallographic orientation of the c-axis of biological apatite as a new index of the quality of subchondral bone in knee joint osteoarthritis, J. Bone Miner. Metab. 35 (2017) 308–314.
[43] J. Wang, T. Ishimoto, T. Nakano, Unloading-induced degradation of the anisotropic arrangement of collagen/apatite in rat femurs, Calcif. Tissue Int. 100 (2017) 87–94.
[44] M. Kashii, J. Hashimoto, T. Nakano, Y. Umakoshi, H. Yoshikawa, Alendronate treatment promotes bone formation with a less anisotropic microstructure during intramembranous ossification in rats, J. Bone Miner. Metab. 26 (2008) 24–33.
[45] Y. Iwasaki, J.J. Kazama, H. Yamato, A. Matsugaki, T. Nakano, M. Fukagawa, Altered material properties are responsible for bone fragility in rats with chronic kidney injury, Bone 81 (2015) 247–254.
[46] T.A. Franz-Odendaal, B.K. Hall, P.E. Witten, Buried alive: how osteoblasts become osteocytes, Dev. Dyn. 235 (2006) 176–190.
[47] M. Zhou, S. Li, J.L. Pathak, Pro-inflammatory cytokines and osteocytes, Curr. Osteoporos. 17 (2019) 97–104.
[48] N. Nishimoto, T. Kishimoto, Humanized antihuman IL-6 receptor antibody, tocilizumab, Handb. Exp. Pharmacol. (2008) 151–160.
[49] S. Kang, T. Tanaka, H. Inoue, C. Ono, S. Hashimoto, Y. Kioi, et al., IL-6 trans-signaling induces plasminogen activator inhibitor-1 from vascular endothelial cells in cytokine release syndrome, Proc. Natl. Acad. Sci. U. S. A. 117 (2020) 22351–22356.
[50] J.T. Sharp, M.D. Lidsky, L.C. Collins, J. Moreland, Methods of scoring the progression of radiologic changes in rheumatoid arthritis. Correlation of radiologic, clinical and laboratory abnormalities, Arthritis Rheum. 14 (1971) 706–720.
[51] D. Van Der Heijde, P. Van Riel, F. Gribnau, I. Nuver-Zwart, L. Van De Putte, Effects of hydroxychloroquine and sulphasalazine on progression of joint damage in rheumatoid arthritis, Lancet 333 (1989) 1036–1038.
[52] H.K. Genant, Y. Jiang, C. Peterfy, Y. Lu, J. Rédei, P.J. Countryman, Assessment of rheumatoid arthritis using a modified scoring method on digitized and original radiographs, Arthritis Rheum. 41 (1998) 1583–1590.
[53] T. Ishimoto, R. Suetoshi, D. Cretin, K. Hagihara, J. Hashimoto, A. Kobayashi, et al., Quantitative ultrasound (QUS) axial transmission method reflects anisotropy in micro-arrangement of apatite crystallites in human long bones: a study with 3-MHz-frequency ultrasound, Bone 127 (2019) 82–90.
[54] L. Knott, A.J. Bailey, Collagen cross-links in mineralizing tissues: a review of their chemistry, function, and clinical relevance, Bone 22 (1998) 181–187.
[55] M. Saito, K. Marumo, Collagen cross-links as a determinant of bone quality: a possible explanation for bone fragility in aging, osteoporosis, and diabetes mellitus, Osteoporos. Int. 21 (2010) 195–214.
[56] L.J.S. da Fonseca, V. Nunes-Souza, M.O.F. Goulart, L.A. Rabelo, Oxidative stress in rheumatoid arthritis: what the future might hold regarding novel biomarkers and add-on therapies, Oxidative Med. Cell. Longev. 14 (2019) 7536805.
[57] Y. Shinno, T. Ishimoto, M. Saito, R. Uemura, M. Arino, K. Marumo, Comprehensive analyses of how tubule occulusion and advanced glycation end-products diminish strength of aged dentin, Sci. Rep. 6 (2016) 19849.
[58] T. Matsuzaka, A. Matsugaki, T. Nakano, Control of osteoblast arrangement by osteocyte mechanoresponse through prostaglandin E2 signaling under oscillatory fluid flow stimuli, Biomaterials 27 (2021), 121203.